Research Article | Vol. 8, No. 7 | 1 Jul 2017 | BIOMEDICAL OPTICS EXPRESS 3470
Biomedical Optics EXPRESS

In vivo multiphoton imaging of a diverse array of fluorophores to investigate deep neurovascular structure

DAVID R. MILLER,[1] AHMED M. HASSAN,[1] JEREMY W. JARRETT,[1] FLOR A. MEDINA,[1] EVAN P. PERILLO,[1] KRISTEN HAGAN,[1] S. M. SHAMS KAZMI,[1] TAYLOR A. CLARK,[2] COLIN T. SULLENDER,[1] THERESA A. JONES,[2] BORIS V. ZEMELMAN,[2] AND ANDREW K. DUNN[1,*]

[1]*Department of Biomedical Engineering, The University of Texas at Austin, 107 W. Dean Keeton C0800, Austin, TX 78712, USA*
[2]*Department of Neuroscience, The University of Texas at Austin, 2415 Speedway, Austin, TX 78712, USA*
[*]*adunn@utexas.edu*

Abstract: We perform high-resolution, non-invasive, *in vivo* deep-tissue imaging of the mouse neocortex using multiphoton microscopy with a high repetition rate optical parametric amplifier laser source tunable between λ=1,100 and 1,400 nm. By combining the high repetition rate (511 kHz) and high pulse energy (400 nJ) of our amplifier laser system, we demonstrate imaging of vasculature labeled with Texas Red and Indocyanine Green, and neurons expressing tdTomato and yellow fluorescent protein. We measure the blood flow speed of a single capillary at a depth of 1.2 mm, and image vasculature to a depth of 1.53 mm with fine axial steps (5 μm) and reasonable acquisition times. The high image quality enabled analysis of vascular morphology at depths to 1.45 mm.

OCIS codes: (180.2520) Fluorescence microscopy; (190.4180) Multiphoton processes; (190.4970) Parametric oscillators and amplifiers.

References and links

1. W. Denk, J. H. Strickler, and W. W. Webb, "Two-photon laser scanning fluorescence microscopy," Science **248**(4951), 73–76 (1990).
2. F. Helmchen and W. Denk, "Deep tissue two-photon microscopy," Nat. Methods **2**(12), 932–940 (2005).
3. J. A. Kubby, *Adaptive Optics for Biological Imaging* (CRC Press, 2013).
4. K. Wang, W. Sun, C. T. Richie, B. K. Harvey, E. Betzig, and N. Ji, "Direct wavefront sensing for high-resolution in vivo imaging in scattering tissue," Nat. Commun. **6**, 7276 (2015).
5. E. Beaurepaire, M. Oheim, and J. Mertz, "Ultra-deep two-photon fluorescence excitation in turbid media." Opt. Commun. **188**, 25–29 (2001).
6. P. Theer, M. T. Hasan, and W. Denk, "Two-photon imaging to a depth of 1000 μm in living brains by use of Ti:Al_2O_3 regenerative amplifier," Opt. Lett. **28**(12), 1022–1024 (2003).
7. D. Kobat, N. G. Horton, and C. Xu, "In vivo two-photon microscopy to 1.6-mm depth in mouse cortex," J. Biomed. Opt. **16**(10), 106014 (2011).
8. N. G. Horton, K. Wang, D. Kobat, C. G. Clark, F. W. Wise, C. B. Schaffer, and C. Xu, "In vivo three-photon microscopy of subcortical structures within an intact mouse brain," Nat. Photonics **7**, 205–209 (2013).
9. D. G. Ouzounov, T. Wang, M. Wang, D. D. Feng, N. G. Horton, J. C. Cruz-Hernández, Y. Cheng, J. Reimer, A. S. Tolias, N. Nishimura, and C. Xu, "In vivo three-photon imaging of activity of GCaMP6-labeled neurons deep in intact mouse brain," Nat. Methods **14**(4), 288–390 (2017).
10. C. Xu, J. Guild, W. W. Webb, and W. Denk, "Determination of absolute two-photon excitation cross sections by in situ second-order autocorrelation," Opt. Lett. **20**(23), 2372–2374 (1995).
11. S. M. S. Kazmi, A. J. Salvaggio, A. D. Estrada, M. A. Hemati, N. K. Shaydyuk, E. Roussakis, T. A. Jones, S. A. Vinogradov, and A. K. Dunn, "Three-dimensional mapping of oxygen tension in cortical arterioles before and after occlusion," Biomed. Opt. Express **4**(7), 1061–1073 (2013).
12. G. Olivié, D. Giguére, F. Vidal, T. Ozaki, J.-C. Kieffer, O. Nada, and I. Brunette, "Wavelength dependence of femtosecond laser ablation threshold of corneal stroma," Opt. Express **16**(6), 4121–4129 (2008).
13. J. Schindelin, I. Arganda-Carreras, E. Frise, V. Kaynig, M. Longair, T. Pietzsch, S. Preibisch, C. Rueden, S. Saalfeld, B. Schmid, J. Tinevez, D. J. White, V. Hartenstein, K. Eliceiri, P. Tomancak, and A. Cardona, "Fiji: an open-source

#287551 https://doi.org/10.1364/BOE.8.003470
Journal © 2017 Received 1 Mar 2017; revised 15 May 2017; accepted 20 Jun 2017; published 28 Jun 2017

Biomedical Optics EXPRESS

platform for biological-image analysis," Nat. Methods **9**(7), 676–682 (2012).
14. J. Ahrens, B. Geveci, C. Law, *ParaView: An End-User Tool for Large Data Visualization* (Elsevier, 2005).
15. E. P. Perillo, J. E. McCracken, D. C. Fernée, J. R. Goldak, F. A. Medina, D. R. Miller, H. C. Yeh, and A. K. Dunn, "Deep in vivo two-photon microscopy with a low cost custom built mode-locked 1060 nm fiber laser," Biomed. Opt. Express **7**(2), 324–334 (2016).
16. L. C. Cheng, N. G. Horton, K. Wang, S. J. Chen, and C. Xu, "Measurements of multiphoton action cross sections for multiphoton microscopy," Biomed. Opt. Express **5**(10), 3427–3433 (2014).
17. M. Berezin, C. Zhan, H. Lee, C. Joo, W. Akers, S. Yazdanfar, and S. Achilefu, "Two-Photon Optical Properties of Near-Infrared Dyes at 1.55 microns Excitation" J. Phys. Chem. B **115**(39), 11530–11535 (2011).
18. M. Drobizhev, N. S. Makarov, S. E. Tillo, T. E. Hughes, and A. Rebane, "Two-photon absorption properties of fluorescent proteins," Nat. Methods **8**(5), 393–399 (2011).
19. P. Tsai, J. P. Kaufhold, P. Blinder, B. Friedman, P. J. Drew, H. J. Karten, P. D. Lyden, and D. Kleinfeld, "Correlations of Neuronal and Microvascular Densities in Murine Cortex Revealed by Direct Counting and Colocalization of Nuclei and Vessels," J. Neurosci. **29**(46), 14553–14570 (2009).
20. J. P. Kaufhold, P. S. Tsai, P. Blinder, and D. Kleinfeld, "Vectorization of optically sectioned brain microvasculature: learning aids completion of vascular graphs by connecting gaps and deleting open-ended segments." Med. Image. Anal. **16**(6), 1241–1258 (2012).
21. D. R. Rivera, C. M. Brown, D. G. Ouzounov, I. Pavlova, D. Kobat, W. W. Webb, and C. Xu, "Compact and flexible raster scanning multiphoton endoscope capable of imaging unstained tissue," P. Natl. Acad. Sci. USA **108**(43), 17598–17603 (2011).
22. S. Khondee and T. D. Wang, "Progress in molecular imaging in endoscopy and endomicroscopy for cancer imaging," J. Healthc. Eng. **4**(1), 1–22 (2013).
23. K. A. Tennant, D. L. Adkins, N. A. Donlan, A. L. Asay, N. Thomas, J. A. Kleim, and T. A. Jones, "The Organization of the Forelimb Representation of the C57BL/6 Mouse Motor Cortex as Defined by Intracortical Microstimulation and Cytoarchitecture," Cereb. Cortex **21**(4), 865–876 (2011).
24. D. Kobat, M. E. Durst, N. Nishimura, A. W. Wong, C. B. Schaffer, and C. Xu, "Deep tissue multiphoton microscopy using longer wavelength excitation," Opt. Express **17**(16), 13354–13364 (2009).

1. Introduction

The ability to visualize deep structures *in vivo* with high spatial resolution is of rising interest to investigate neuronal physiology and cerebral vasculature. Optical imaging offers non-invasive, high-resolution *in vivo* microscopy techniques to observe brain tissue and its surrounding environment. Confocal fluorescence microscopy using one-photon excitation is limited to imaging the superficial tissue surface due to the scattering of short excitation wavelength light in heterogeneous brain tissue. To overcome depth limitations, nonlinear multiphoton excitation is widely used. Two-photon fluorescence laser-scanning microscopy (2PM), developed in the early 1990's [1], uses an ultrafast laser to cause two-photon excitation of a fluorophore in a confined excitation volume. An image is formed by scanning a focused laser beam across a sample as fluorescence is detected. Conventional 2PM is performed with titanium-doped sapphire (Ti:S) oscillators because of their reliability to output mode-locked femtosecond pulses with high average power. Ti:S oscillators provide a tunable excitation wavelength between 700 and 1,000 nm, which covers the peak two-photon absorption of a myriad of common fluorophores. 2PM performed with Ti:S oscillators has been shown to reach a maximum imaging depth of 800 μm in the neocortex [2].

Despite the ability of 2PM to restrict fluorescence to a confined focal volume and improve access to deeper anatomical layers, maximum imaging depth still remains limited by the effects of scattering. Various strategies exist to mitigate scattering effects to further extend the imaging depth of *in vivo* 2PM. A recent strategy is to shape the wavefront of the excitation light with adaptive optics to minimize aberrations incurred by scattering in the tissue [3]. Wang et al. demonstrated wavefront sensing to a depth of 700 μm in mouse cortex [4]. A second strategy is to use higher energy pulses on the order of microjoules which results in more photons reaching the excitation volume at greater tissue depths [5]. Theer et al. demonstrated an imaging depth of 1,000 μm using a regeneratively amplified Ti:S oscillator at a center wavelength of 925 nm and repetition rate of 200 kHz [6]. A third strategy is to use oscillators with longer excitation wavelengths to reduce the effects of scattering by tissue. At wavelengths beyond 1,000 nm, a

Biomedical Optics EXPRESS

fluorophore may undergo either two-photon excitation (2PE) or three-photon excitation (3PE) depending on the fluorophore's absorption properties. Deep-tissue imaging has been demonstrated with both 2PE and 3PE. Kobat et al. demonstrated an imaging depth of 1.6 mm using 1,280 nm excitation light with 1.5 nJ pulse energy (80 MHz repetition rate) to cause 2PE of Alexa680 [7]. A fourth approach is to use both high energy pulses and longer excitation wavelengths; however, higher energy pulses come at the expense of a reduced repetition rate. Horton et al. demonstrated an imaging depth of 1.4 mm with a soliton self-frequency shifted fiber laser at 1,700 nm with a 67 nJ pulse energy (1 MHz repetition rate) to cause 3PE of Texas Red [8]. Ouzounov et al. recorded spontaneous activity from GCaMP6-labeled neurons in the hippocampus at a depth of 1 mm using a noncolinear optical parametric amplifier at 1,300 nm with a 1,250 nJ pulse energy (400 kHz repetition rate) [9].

In this paper, we take the approach of using both high energy pulses and longer excitation wavelength with an increased laser repetition rate to achieve fast image acquisition. We demonstrate routine *in vivo* deep-tissue multiphoton imaging in mouse cortex using an optical parametric amplifier (OPA) that is tunable between 1,100 and 1,400 nm with an output pulse energy of 400 nJ and a repetition rate of 511 kHz. The tunability of the OPA across a wide spectrum enables efficient excitation of many common fluorophores. Unfortunately, the brightness of many common fluorophores has not been characterized near 1,300 nm, thus we measure the cross sections of both Texas Red and Indocyanine green (ICG) across the OPA spectrum to determine their optimal excitation wavelengths. We demonstrate deep-tissue imaging of vasculature labeled with Texas Red and ICG, and neurons expressing tdTomato and yellow fluorescent protein (YFP). The combined high repetition rate (511 kHz) and high pulse energy (400 nJ) of the OPA enables fast image acquisition due to the increased signal-to-background ratio (SBR) with a single laser pulse. This allows for entire stacks (even beyond 1 mm) to be acquired with small axial step sizes (5 μm) to achieve fluid 3D reconstruction of vessels and neurons.

2. Materials and methods

2.1. Multiphoton microscope and laser design

The multiphoton microscope and laser setup is shown in Fig. 1(a). A λ=800 nm mode-locked Ti:S oscillator (Mira 900, Coherent) is externally stretched to seed a regenerative amplifier (RegA 9000, Coherent) that is custom-modified to operate at a tunable repetition rate up to 511 kHz. The seed pulse is amplified to a pulse energy of 6 μJ (average power of 3 W at 511 kHz) and then externally compressed to a pulse width of 105 fs. Next, the compressed 800 nm high-energy pulse is converted to a longer wavelength by an OPA (OPA 9800, Coherent) that is tunable between 1,100 and 1,400 nm with a maximum pulse energy of 400 nJ at 511 kHz. The OPA output is pre-chirped by a pair of prisms before entering the microscope such that the pulse is nearly Fourier-transform limited at the focus of the microscope objective. The temporal pulse width at the focus of the microscope objective is τ=42 femtoseconds as measured by *in situ* second order autocorrelation [10], as shown in Fig. 1(b). Figure 1(c) shows the OPA spectrum used for imaging tdTomato (λ=1,140 nm), Texas Red (λ=1,215 nm), Texas Red and YFP simultaneously (λ=1,280 nm), and ICG (λ=1,350 nm).

Imaging was performed on a custom-built upright multiphoton microscope system [11]. The laser was scanned with an xy-galvanometer mirror pair (6125H, Cambridge Technologies), and then expanded via a Plössl scan lens (40 mm) and tube lens (200 mm) to fill the back aperture of the microscope objective (XLPLN25XSVMP2 from Olympus for imaging Texas Red, ICG, and YFP; XLUMPLFLN 20X 0.95 NA from Olympus for imaging tdTomato). Heavy water was used as the immersion medium to reduce absorption of the OPA excitation light. Fluorescence was epi-collected and directed to the detector by a dichroic mirror. For imaging Texas Red and tdTomato, we used a dichroic with a cutoff at 775 nm (FF775-Di01-52x58, Semrock) and photomultiplier tube (PMT) with peak sensitivity at λ=580 nm (H10770PB-40, Hamamatsu

Biomedical Optics EXPRESS

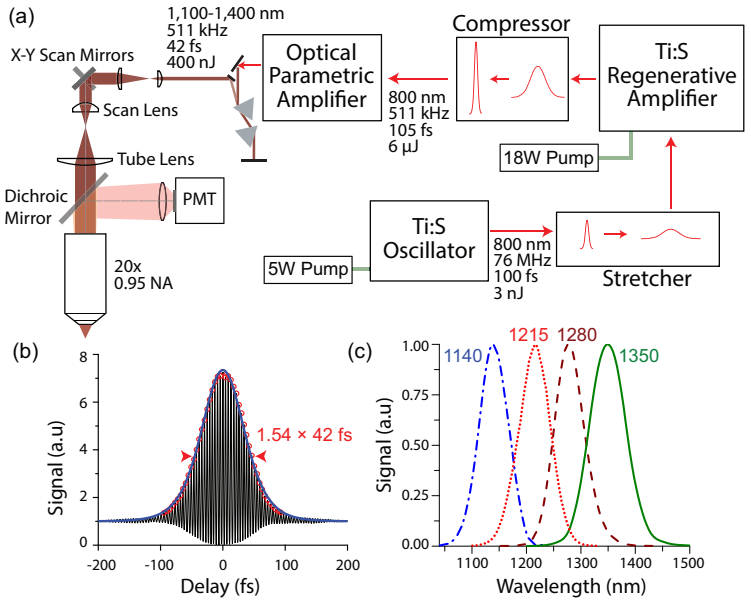

Fig. 1. (a) Schematic of laser and microscope design. A Ti:S oscillator seeds a regenerative amplifier, which is tunable up to 511 kHz. The amplified pulse is converted to a longer wavelength by an optical parametric amplifier (OPA). The OPA output pulse is tunable between 1,100 nm and 1,400 nm and has a maximum pulse energy of 400 nJ at 511 kHz. (b) Interferometric autocorrelation trace of the OPA pulse after the microscope objective; red dots indicate peaks of the autocorrelation trace and the blue line is a $\mathrm{sech}^2(t)$ fit to the autocorrelation envelope. The measured temporal pulse width of the OPA was τ=42 femtoseconds. (c) Spectrum of OPA for imaging tdTomato at 1,140 nm, Texas Red at 1,215 nm, Texas Red and YFP simultaneously at 1,280 nm, and ICG at 1,350 nm.

Photonics). For imaging ICG, we used a dichroic with a cutoff at 875 nm (FF875-Di01-52x58, Semrock) and PMT with peak sensitivity at λ=800 nm (H10770PB-50, Hamamatsu Photonics). Custom software controlled the image acquisition. All frames are 512 × 512 pixels, and all stacks are in 5 μm depth increments. Appropriate emission filters were placed in front of the PMT. For imaging Texas Red, we used a 750 nm short pass filter (FF01-750/SP-25, Semrock) and 610 nm band pass filter (HQ/610/75M, Chroma). For imaging ICG, we used a 830 nm bandpass filter (RT-830, Edmund Optics). For imaging tdTomato, we used a 750 nm short pass filter and 609 nm band pass filter (FF01-609/181-25, Semrock). For imaging Texas Red and YFP simultaneously, we used the aforementioned parameters for Texas Red and added another channel in the collection arm to separate the YFP fluorescence. For imaging YFP, we used a 680 nm short pass filter (FF01-680/SP-25, Semrock) and 510 nm band pass filter (FF01-510/84-25, Semrock). The laser power was adjusted throughout each stack with a computer-controlled, rotating half-wave plate and polarizing beam splitter; we maintained a pulse energy below 20 nJ at the focus to ensure sample damage did not occur [12]. We observed no damage to vasculature or neurons and were able to image the mice chronically. Rendering of three-dimensional (3D) stacks was performed with visualization software (Avizo, Fiji [13], and ParaView [14]).

2.2. *Animal preparation*

All animal procedures were approved by The University of Texas at Austin Institutional Animal Care and Use Committee. We prepared cranial window implants in C57 mice and left the dura

Biomedical Optics EXPRESS

intact as described in [15] (we note that for imaging Texas Red and YFP simultaneously, we used thy1-YFP-H mice from Jackson Laboratory expressing YFP in motor and sensory neurons, particularly layer V pyramidal cells). Mice were anesthetized with isoflurane throughout surgery and imaging. Body temperature was maintained at 37.5° Celsius, and 0.1 mL subcutaneous injections of 5% (w/v) glucose in physiological saline were applied every 2 hours. For imaging Texas Red and ICG, a retro-oribtal injection of the fluorescent dye was performed to label blood plasma in the vasculature. For imaging tdTomato, neurons were labeled by cortical injection of adeno-associated viral vectors carrying a tdTomato plasmid. Imaging sessions were performed a week following the delivery of the viral vectors.

2.3. Characterization of fluorophores

To maximize imaging depth, it is important to excite a fluorophore at or near its absorption peak. Two-photon absorption spectra were not previously reported for either Texas Red or ICG, thus we characterized the absorption spectra of both Texas Red and ICG across the OPA tuning range. First, we dissolved Texas Red (Thermo Fisher Scientific) in saline and placed 0.5 mL of a 48 μM solution into a cuvette. Similarly, we dissolved ICG (Sigma-Aldrich) in a 5% bovine serum albumin-saline solution and placed 0.5 mL of a 100 μM solution into a cuvette. The concentrations of Texas Red and ICG was determined via spectrophotometry (UV-3600, Shimadzu) using known extinction coefficients. We then measured the fluorescence from each cuvette using our setup shown in Fig. 1(a) replacing the objective with one with a smaller back aperture (CFI Plan 10X/0.25 NA, Nikon) to ensure the objective focus in the cuvette was diffraction-limited and added a photon counter (DPC-230, Becker and Hickl) to measure the number of fluorescent photons detected by the PMT. We then measured the dependence of Texas Red and ICG fluorescence on excitation power to determine whether the fluorescence was the result of 2PE or 3PE. For these measurements, the excitation power was increased from about 0.3 mW to 1 mW. Next, we measured the cross sections of Texas Red and ICG with the same setup. For these measurements, 1 mW of power or less was used to ensure the same power range as the power dependence measurements. Following the methods outlined in Cheng et al., we measured the absolute action cross section of Texas Red using their reported value of 20.6 GM as the two-photon action cross section of SR101 at 800 nm to calculate the collection efficiency for Texas Red in our system, since SR101 and Texas Red have very similar emission spectra [16]. We measured the relative cross section for ICG but were unable to measure the absolute cross section due to the absence of a dye with a known cross section and similar emission spectra to ICG. However, we note that Berezin et al. measured ICG in water to have a two-photon action cross section of 6.3 GM at 1.55 μm excitation [17]. We also measured the dependence of YFP fluorescence on excitation power using a thy1-YFP-H mouse brain slice. We did not characterize tdTomato since previous work by Drobizhev et al. demonstrated that tdTomato has a two-photon cross section of about 30 GM at 1,140 nm [18].

3. Experimental results

3.1. In vivo multiphoton microscopy imaging

Two-photon microscopy images of vasculature were separately acquired in different mice using two fluorescent dyes – Texas Red and ICG. Figure 2(a) demonstrates an imaging depth of 1,535 μm for vasculature labeled with Texas Red (see Visualization 1 for fly-through of entire z-stack). We are able to acquire the stack in 5 μm depth increments because we perform reasonable averaging (3 frames from 0 to 500 μm, 5 frames from 500 to 700 μm, 7 frames from 700 to 900 μm, 9 frames from 900 to 1,100 μm, 11 frames from 1,100 to 1,300 μm, 14 frames from 1,300 to 1,400 μm, 16 frames from 1,400 to 1,500 μm, and 24 frames from 1,500 to 1,535 μm) and image at a fast frame rate of 1.58 Hz. We attribute our minimal averaging, even at

Biomedical Optics EXPRESS

depths greaten than 1,000 μm, to the high pulse energy of the OPA. The excitation power was increased to maintain similar signal levels down to 1,000 μm, at which point we reached full power equating to 122 mW at the sample surface (transmission of the 25X objective at 1,215 nm is 67%). All frames were normalized individually. In Fig. 2(b), individual blood vessels can be seen with high contrast beyond 1,000 μm and still resolved beyond 1,350 μm. Figure 2(c) demonstrates our ability to measure blood flow velocity in individual capillaries at an imaging depth of 1,200 μm. The highlighted red line (top) indicates the position of the line scan (bottom). To the best of our knowledge, this is the deepest line scan performed *in vivo* to date. The blood flow speed was measured to be 1.1 ± 0.1 mm/s.

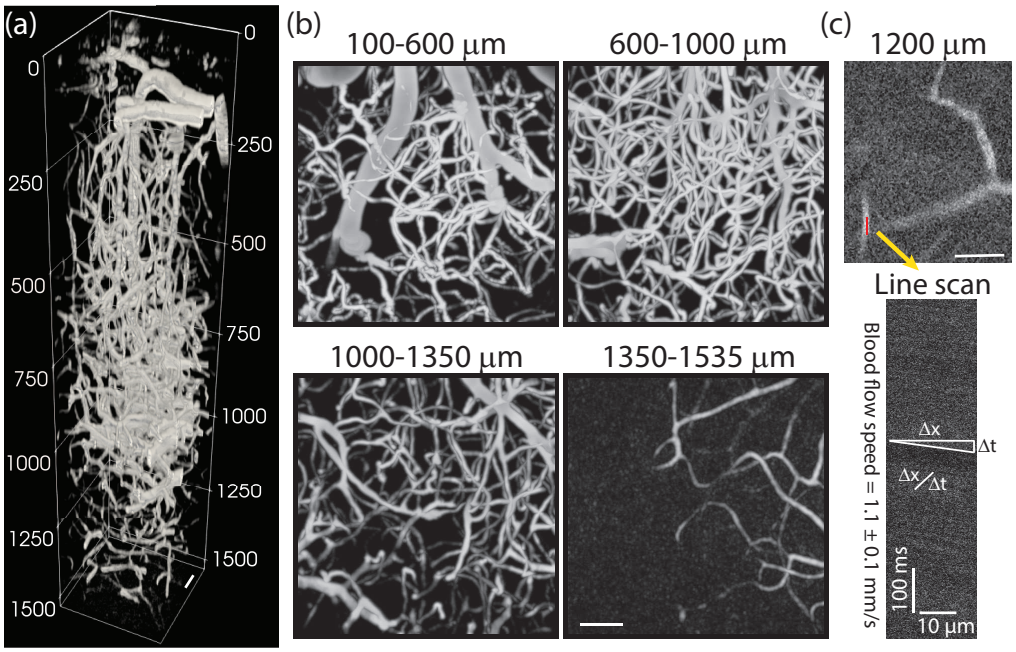

Fig. 2. *In vivo* two-photon microscopy images of vasculature labeled with Texas Red. (a) Three-dimensional reconstruction of a 1,535 μm stack. (b) x-y intensity projections of stack shown in (a). (c) (top) x-y intensity projection at depth of 1200 μm (note: image from different stack than shown in (a)). A line scan was performed at the highlighted red line. (bottom) Line scan at depth of 1200 μm. All scale bars are 50 μm unless otherwise indicated.

In order to quantify the benefits of our high repetition rate excitation source, SBR analysis was performed at various imaging depths and laser repetition rates. For these measurements, the SBR was calculated from line profiles taken through vessels. Figure 3(a) compares the highest SBR value obtained at depths of 100, 300, 600, and 940 μm for repetition rates of 511 (red) and 255 kHz (blue). As the imaging depth increases, the benefits of a 511 versus 255 kHz repetition rate become apparent as an improvement by more than a factor of $\sqrt{2}$ arises. Figure 3(b) compares the SBR of a vessel at z=940 μm for imaging with a laser repetition rate of 511 kHz versus 255 kHz (the sampling rate was synchronized with the respective laser repetition rate). The raw images of the vessel for imaging at both 511 kHz and 255 kHz were averaged over 10 frames, and the yellow line indicates a 6 μm thick line over which the SBR was calculated. The line profile shows that the SBR is 12.0 for imaging at 511 kHz, and 5.5 for imaging at 255 kHz. Figure 3(c) shows the normalized intensity profile for a line through a blood vessel (indicated by yellow line) at a depth of z=1,430 μm for the stack shown in Fig. 2. The dotted line indicates the background value calculated by averaging pixel values outside of the

Biomedical Optics EXPRESS

vessel. A 1 pixel median filter was applied to the image before taking the line profile, however the image histogram was not stretched. The calculated SBR is 2.09. Due to the high SBR of the deep image data and the rapid stack acquisition at fine axial steps, the vascular network could be vectorized using Volumetric Image Data Analysis [19, 20]. Figure 3(d) depicts these results as centerlines of vessels from 1,200 to 1,450 μm for the stack shown in Fig. 2 overlaid on the maximum intensity projection of the raw data from 1,200 to 1,450 μm. The color of the centerlines encodes for depth according to the color map.

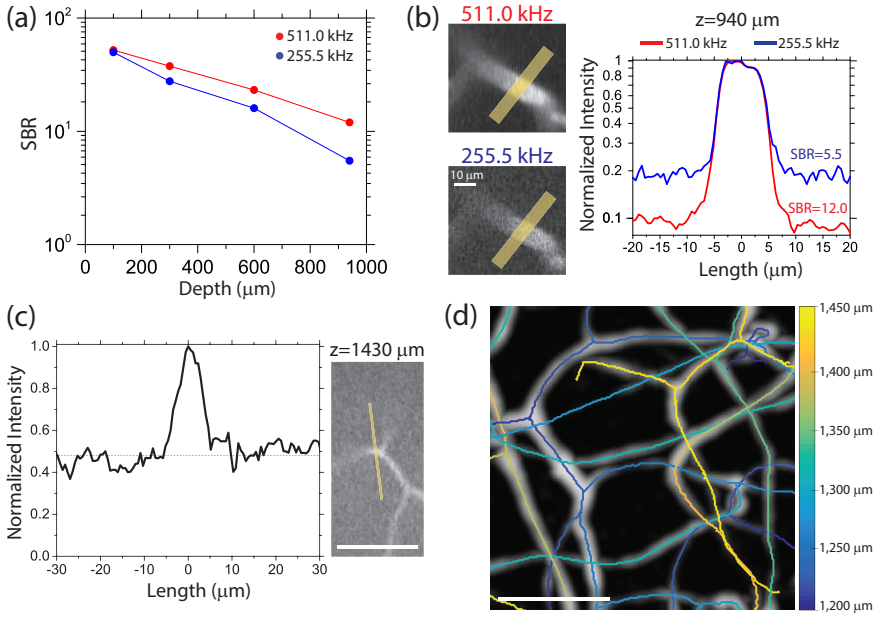

Fig. 3. (a) The SBR as a function of depth for a laser repetition rate of 511 kHz (red) and 255 kHz (blue). The lines serve as guides for the eye. (b) Comparison of the SBR for a vessel at z=940 μm for laser repetition rates of 511 and 255 kHz. The vessel images are a 10-frame average at the respective repetition rate; the images are shown at full scale. The line profile is averaged over a 6 μm line indicated by the yellow lines in the vessel images. (c) Normalized intensity profile for a line through a blood vessel at z=1430 μm, demonstrating a SBR above 2 (the dotted black line indicates the calculated background). The yellow line on the vessel image, which is a 16-frame average, indicates where the line profile was taken. (d) Centerlines of vessels from 1,200 to 1,450 μm depth encoded by color . The centerlines are overlaid on a maximum intensity projection of the raw data from Fig. 2. All scale bars are 50 μm unless otherwise indicated.

Due to the tunability of our excitation source, our imaging system is also able to excite other far-red fluorescent dyes. Figure 4(a) shows a 3D rendering of vasculature labeled with ICG to an imaging depth of 1,000 μm (see Visualization 2 for entire z-stack). Excitation power at λ=1,350 nm was increased to maintain similar signal levels down to 750 μm at which point we reached full power equating to 58 mW at the sample surface (the transmission of the 25X objective at 1,350 nm is 74%). All frames throughout the stack were normalized individually. Figure 4(b) shows x-y intensity projections from another stack in a different mouse in which we also reached 1,000 μm in depth, thus demonstrating the repeatability of two-photon imaging with ICG. Individual vessels can be seen with high contrast throughout the entire stack. ICG is FDA approved for human use and is commonly used for ICG angiography in ophthalmology. Its far-red fluorescence emission near 830 nm makes it an ideal candidate for translating deep-

Biomedical Optics EXPRESS

tissue multiphoton microscopy to clinical applications [21, 22].

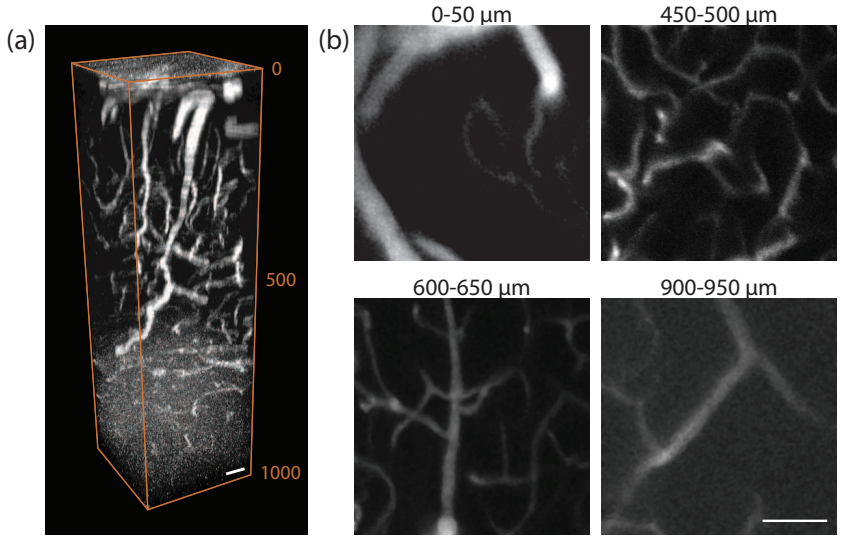

Fig. 4. *In vivo* two-photon microscopy images of vasculature labeled with ICG. (a) Three-dimensional reconstruction of a 1,000 μm stack. (b) x-y intensity projections from another mouse. All scale bars are 50 μm.

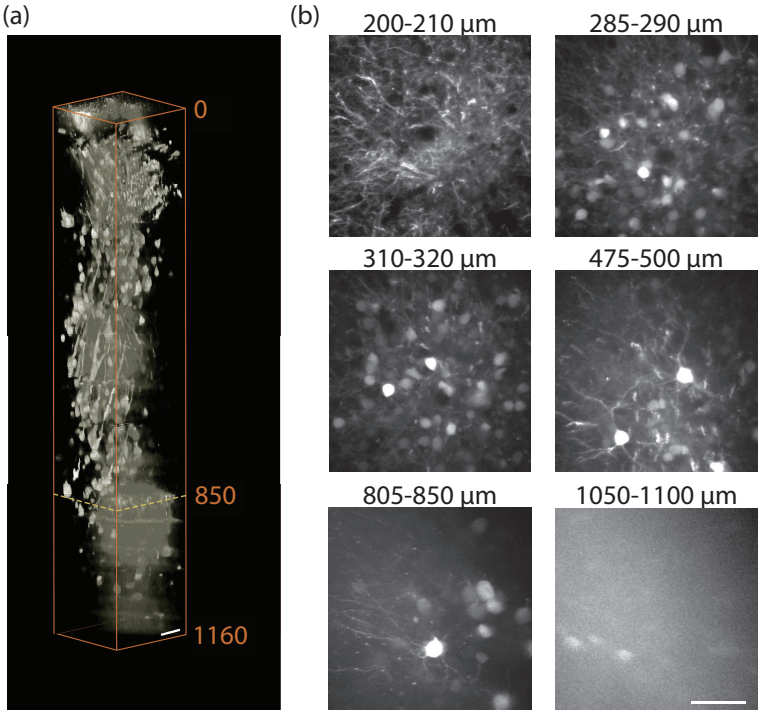

Fig. 5. In vivo two-photon microscopy images of neurons labeled with tdTomato. (a) Three-dimensional reconstruction of a 1,160 μm stack of neurons within a mouse brain. (b) x-y intensity projections from stack shown in (a). All scale bars are 50 μm.

Biomedical Optics EXPRESS

In addition to imaging vasculature perfused with fluorescent dyes, we can also image neurons expressing a range of different fluorescent proteins. Figure 5(a) demonstrates an imaging depth of 1,160 μm in neurons expressing tdTomato. Excitation power was increased to maintain similar signal levels down to 850 μm at which point we reached full power equating to 40 mW at the sample surface (the transmission of the 20X objective at 1,140 nm is 52%). The yellow dotted line signifies the reference plane for which all frames below were normalized; all frames above were normalized individually. The delivery of the tdTomato plasmid causes a 200 μm $\times$ 200 μm transverse area of expression after a week following injection. The expression is strongest in the center of the transverse area, which is why the 3D reconstruction in Fig. 5(a) appears saturated in the transverse center. Individual neuron bodies are visible throughout the stack, as shown in the x-y intensity projections in Fig. 5(b) (see Visualization 3 for entire z-stack).

The imaging results presented in Figs. 2-5 were acquired at imaging sites 2.5 mm posterior and 2.5 mm lateral to the bregma. To investigate deep-tissue imaging closer to the bregma, we performed simultaneous imaging of Texas Red and YFP at a site 0.25 mm anterior and 1.5 mm lateral to the bregma, which is the most responsive forelimb region of the motor cortex [23]. Figure 6(a) shows a laser speckle contrast image of the mouse craniotomy - the red square indicates the two-photon imaging location. The bottom of Fig. 6(a) is a 300 $\times$ 300 $\times$ 400 μm^3 two-photon maximum intensity projection of the surface vasculature outlined by the red square. Figure 6(b) is an x-z intensity projection for a 1,330 μm stack acquired at the site outlined by the red square in Fig. 6(a). The vasculature (red) can be seen throughout the stack and the neurons (green) can be traced down to their cell bodies in layer V (see Visualization 4 for entire z-stack of vasculature and neurons). The top image of Fig. 6(c) is an x-y intensity projection showing the neuron cell bodies in layer V (green) overlaid with the microvasculature (red). The bottom image of Fig. 6(c) depicts a vessel at an imaging depth of 1,330 μm. Taken together with Figs. 2-5, these results demonstrate our ability to routinely obtain high quality images of vessels and neurons labeled with a variety of fluorescent dyes and proteins deep in mouse brain tissue.

3.2. *Cross section spectra of Texas Red and ICG*

Power dependence measurements for Texas Red, ICG, and YFP are shown in Fig. 7(a). Near an excitation wavelength of 1,350 nm, ICG undergoes 2PE as indicated by a slope of 2.03. Near an excitation wavelength of 1,280 nm, Texas Red undergoes 2PE as indicated by a slope of 1.97. We note that Texas Red can undergo both 2PE and 3PE at higher excitation powers. However, for the imaging experiments with Texas Red shown in Figs. 2 and 6, we expect that the excitation power at the samples focus is in the 2PE regime. Near an excitation wavelength of 1,280 nm, YFP undergoes 3PE as indicated by a slope of 3.00. Figure 7(b) shows the two-photon action cross section of Texas Red from 1,150 to 1,360 nm. Figure 7(c) shows the relative two-photon cross section of ICG from 1,200 to 1,450 nm. The estimated uncertainty for the measurements is 30%. We chose excitation wavelengths for imaging Texas Red, ICG, tdTomato, and YFP, respectively, as a compromise between maximizing the attenuation length in brain tissue, fluorophore brightness, and laser power.

4. Discussion

There are two advantages of our laser system for deep imaging. First, the OPA wavelength can be tuned to match the peak two- or three-photon absorption of the target fluorophore. The wide tuning range allows for the excitation of numerous different fluorophores, as demonstrated in this paper. Unfortunately, few fluorophores have been characterized for excitation wavelengths beyond 1,100 nm. We characterized the brightness of Texas Red and ICG, though neither are exceptionally bright fluorophores at the evaluated wavelengths. Imaging depth could be significantly improved with the development and characterization of new fluorophores that are

Biomedical Optics EXPRESS

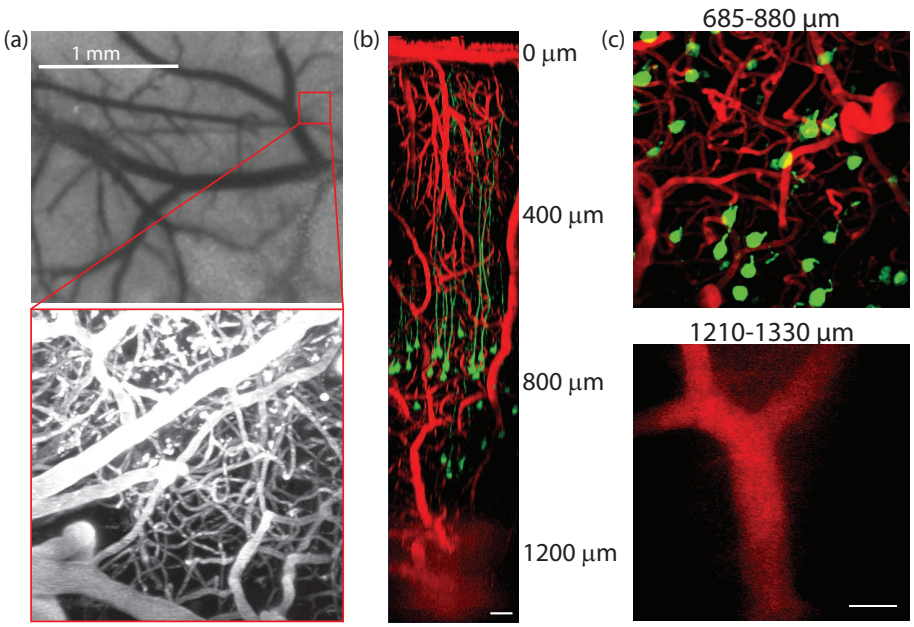

Fig. 6. *In vivo* two-photon microscopy images of vasculature labeled with Texas Red and neurons labeled with YFP. (a) Laser speckle contrast image of mouse craniotomy. The red square indicates the two-photon imaging location. The zoomed view is a 300 × 300 × 400 μm^3 two-photon maximum intensity projection. (b) x-z intensity projection of a 1,330 μm stack of vasculature (red) and neurons (green). (c) x-y intensity projections of stack shown in (b) demonstrating neuron cell bodies in layer V and a large blood vessel at a depth of 1,330 μm. All scale bars are 50 μm unless otherwise indicated.

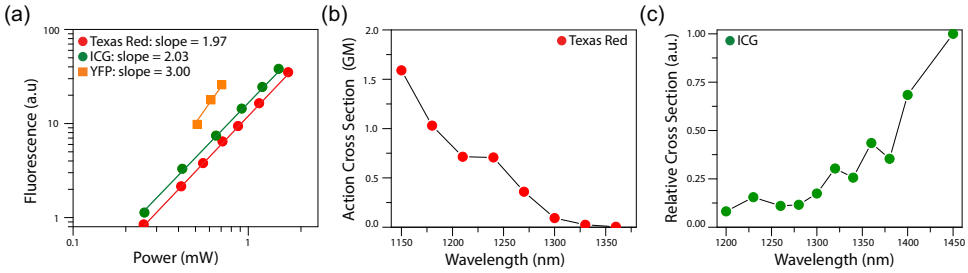

Fig. 7. Characterization of Texas Red, ICG, and YFP. (a) Logarithmic power dependence plot for ICG, Texas Red, and YFP. ICG undergoes two-photon excitation at 1,350 nm indicated by a slope of 2.03. Texas Red undergoes two-photon excitation at 1,280 nm as indicated by a slope of 1.97. YFP undergoes three-photon excitation at 1,280 nm as indicated by a slope of 3.00. Note that the power was measured after the objective. (b) Two-photon action cross section of Texas Red in units of Goeppert-Mayer (GM). Solid line serves as a guide to the eye. (c) Relative two-photon cross section of ICG. Solid line serves as a guide to the eye.

Biomedical Optics EXPRESS

optimized to have their peak two-photon absorption near 1,300 nm at which the attenuation length in mouse brain cortex is maximized. Additionally, it would be advantageous for these fluorophores to have red-shifted emission spectra (similar to that of ICG) to reduce the attenuation of fluorescent photons traveling from the excitation volume to the microscope objective. Future work will aim to identify and characterize fluorescent dyes that are both brighter near an excitation of 1,300 nm and more cost-effective. Texas Red is an affordable option for deep imaging near 1,300 nm but not extremely bright, while Alexa680 is significantly brighter [24] but more expensive.

Second, our regenerative amplifier can operate at a repetition rate up to 511 kHz while maintaining the same pulse energy as at lower repetition rates. Ti:sapphire based regenerative amplifiers typically used in other literature for multiphoton microscopy run at repetition rates at or below 250 kHz [5, 6]. Running at a faster repetition rate while maintaining a high pulse energy enables faster image acquisition and better signal-to-noise ratio. We demonstrate this in Fig. 3 for which we determined there is an approximate $\sqrt{2}$ gain in SBR by doubling the repetition rate for depths between 300 and 600 μm, and interestingly, an even greater gain at deeper depths.

The advantages of our system - the ability to tune the excitation wavelength and operate at a high repetition rate - add significant cost and complexity to the laser system. Many laboratories and clinics may prefer a simpler system that is more affordable and easier to use, though these systems typically lack the ability to tune the excitation light source. However, the cost and complexity enables new investigations into vascular morphology and dynamics. For example, we demonstrate an imaging depth beyond 1.5 mm (shown in Fig. 2) with 5 μm axial steps. Using fine axial steps, we capture the continuous changes of vasculature morphology and can track the centerlines of the vessels throughout the stack (shown in Fig. 3(a)). Another group has reached similar depths - 1.6 mm using 1,280 nm excitation light at 80 MHz (1.5 nJ pulse energy) to excite Alexa680 [7] - however, they average up to 224 frames to account for the low pulse energy and take 20 μm axial step sizes in order to capture the stack in a practical time limit. Large frame averaging and z-step sizes are not a practical method to chronically study vascular dynamics and morphology.

We are also able to discern functional information about the vasculature at depths beyond 1 mm. We determined the blood flow speed in a single vessel at a depth of 1.2 mm (shown in Fig. 2(c)), which can be useful for characterizing the health of blood vessels. The deepest previously reported line scan was at a depth of 900 μm performed with a 82 MHz oscillator at 1,280 nm [24]; since line scans must be performed with little to no averaging in order to capture the dynamics of blood flow, a high pulse energy laser like the OPA is able to achieve better SBR in deep tissue and thus record deeper line scans.

An important consideration in choosing a fluorescent dye to label vasculature is the clearance time of the dye. Ideally, a dye would maintain a similar concentration in the blood plasma for the duration of an imaging session. However, dyes that clear quickly may limit the maximum pixel dwell time and frame averaging. We found that ICG was significantly cleared after 30 minutes which severely limited frame averaging throughout a deep imaging stack. We performed a 6 frame average from 0 to 400 μm below the surface, 12 frame average from 400 to 750 μm, and 15 frame average from 750 to 1,000 μm for the 3D reconstruction in Fig. 4(a). Thus, the ICG dye was nearly cleared during the acquisition of the stack from about 700 μm to 1,000 μm which resulted in poor signal at these depths. We found that it took approximately 90 minutes for Texas Red to clear, allowing us to average for 3 frames from 0 to 500 μm, 5 frames from 500 to 700 μm, 7 frames from 700 to 900 μm, 9 frames from 900 to 1,100 μm, 11 frames from 1,100 to 1,300 μm, 14 frames from 1,300 to 1,400 μm, 16 frames from 1,400 to 1,500 μm, and 24 frames from 1,500 to 1,535 μm for the 3D reconstruction in Fig. 2(a). For the 3D reconstruction in Fig. 6(b), we averaged for 3 frames from 0 to 745 μm, 6 frames from 750 to 1,000 μm, 12 frames from 1,000 to 1,300 μm, and 18 frames from 1,300 to 1,330 μm. Fluorescent proteins

Biomedical Optics EXPRESS

like tdTomato have the advantage that they are not cleared, and they are typically much brighter than fluorescent dyes. For the 3D reconstruction of neurons labeled with tdTomato in Fig. 5(a), we averaged for 5 frames from 0 to 800 μm, 8 frames from 800 to 900 μm, 20 frames from 900 to 1,000 μm, and 25 frames from 1,000 to 1,160 μm.

5. Conclusion

We have demonstrated that a high pulse energy (400 nJ) light source with a high repetition rate (511 kHz) that is tunable between 1,100 and 1,400 nm can extend the imaging depth of traditional 2PM and excite a variety of fluorescent dyes and proteins deep in mouse cortex. We show imaging depths of 1.53 mm for vasculature labeled with Texas Red and 1.16 mm for neurons labeled with tdTomato. We also demonstrate vascular imaging with ICG (an FDA approved fluorescent dye), neuron imaging with YFP, and measure blood flow speed at a depth of 1.2 mm. The high repetition rate and high pulse energy of the OPA laser system produces high image quality with reasonable image acquisition times and fine axial steps for deep stacks, enabling the analysis of vascular morphology at depths to 1.45 mm.

Funding

National Institutes of Health (NS082518, NS078791, EB011556); American Heart Association (14EIA18970041); Cancer Prevention and Research Institute of Texas (RR160005); D.R.M. is supported by the National Science Foundation Graduate Research Fellowship Program (DGE-1110007).